

# Jackiw-Rebbi-type bound state carrying fractional fermion parity

Ye Xiong

*Department of Physics and Institute of Theoretical Physics ,  
Nanjing Normal University, Nanjing 210023, P. R. China\**

Peiqing Tong

*Department of Physics and Institute of Theoretical Physics ,  
Nanjing Normal University, Nanjing 210046, P. R. China  
Jiangsu Key Laboratory for Numerical Simulation of Large Scale Complex Systems,  
Nanjing Normal University, Nanjing 210023, P. R. China and  
Kavli Institute for Theoretical Physics China, CAS, Beijing 100190, China<sup>†</sup>*

We find the coexistence of two kinds of non-abelian anyons, Majorana fermion at the geometric ends and Jackiw-Rebbi-type bound state (JRBS) at a domain-wall, in a topological superconducting phase in one-dimensional (1D) systems. Each localized JRBS carries a new fractional quantity, half of the parity of fermion number. This induces a topological protected crossing at the zero energy for its eigen-energy. For a chain embedded with a JRBS, one is possible to switch between the occupied and empty states of Majorana zero energy state (MZES) by varying the strength of external magnetic field across that crossing point. This enable a way to encode a quantum qubit into one MZES without breaking parity conservation. We propose that such JRBS and Majorana fermion can appear in two 1D models, one can be accomplished in an artificial lattice with staggered hopping, staggered spin-orbital interaction and staggered superconducting pairing for cold fermion atoms, the other is describing a 1D semiconductor chain sandwiched between s-wave superconductor and antiferromagnet.

PACS numbers: 73.63.Nm, 74.45.+c, 14.80.Va, 75.60.Ch

*Introduction.*— It has been proposed that Majorana Fermions (MF) can exist in a topological superconducting phase (TSP) at the core of magnetic vortex penetrating a 2-dimensional (2D)  $p_x \pm ip_y$  superconductor[1–9] or at the ends of a 1-dimensional (1D)  $p$  wave superconductor [5, 10–15]. These MFs, being their own anti-particles, obey non-abelian braiding statistics so that the quantum computing based on them is fault-tolerant [3, 16]. In practice, a quantum qubit is encoded into two Majorana zero energy states (MZES) but not into one because the parity conservation prevents the switching between the occupied and empty states of a MZES. This restriction definitely increases the complexity of the topological computing in experiment.

In this paper, by considering the coexistent Jackiw-Rebbi-type bound state (JRBS) on a domain-wall[12, 13, 17–20], we are able to switch between the occupied and empty states of a MZES by varying external magnetic field. This switching manipulation is based on a topologically protected crossing at the zero energy for the eigen-energy of JRBS, which has been schematically showed in Fig. 1(b).

At the first glance, it is surprising that a localized JRBS can affect the global properties encoded in MZES. The key clue is that in the present of superconducting coupling, JRBS has abandoned one of its well-known properties: each JRBS carries fractional charge  $e/2$  [12, 17]. This is due to the broken of fermion number conservation. But the parity conservation of fermion number is still present which makes JRBS carry fractional par-

ity(FP), a fractional quantity used to hide behind fractional charge. It is in this way that the localized JRBS links with the global property, parity of total fermion number.

Firstly we want to illustrate how FP occurs in the 1D systems. Suppose there are two infinite chains, A and B. A is uniform and B has a pair of JRBSs and is uniform elsewhere. The parameters on A and B are the same. The two JRBSs on B are far from each other so that each one can be considered individually. In the absence of superconducting pairing, the total numbers of fermions are well defined, denoted as  $N_A$  and  $N_B$  in the chains A and B respectively. A standard Thouless pump tells us that the two JRBSs in B cause  $|N_A - N_B| = 1$ . The fractional charge  $e/2$  carried by JRBS is produced in this argument because each JRBS must take the responsibility of the half of one elemental charge induced by the fermion number difference. When the superconducting pairing is nonzero, the conserved quantities on the chains, A and B, regress from fermion number to fermion parity,  $P_{A(B)} = N_{A(B)} \bmod 2$ . We will show that the well defined (conserved) quantities on A and B are different by  $|P_A - P_B| = 1$ . So each JRBS takes the responsibility of the half of this parity difference. This is the source from where the concept, FP, comes.

We will also show that this feature could be realized in two 1D systems showed in Fig. 1 (a). The first model can be realized with cold atoms in an artificial 1D lattice with staggered nearest neighboring hopping, staggered spin orbital interaction and staggered superconducting

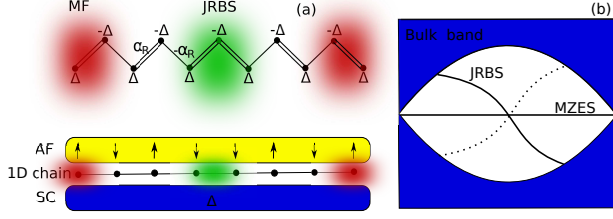


FIG. 1: (Color online) (a) two 1D models we studied. In the upper model, the double bonds and single bond are used to illustrate the alternative stronger and weaker hoppings between the nearest neighboring sites. The spin-orbital interaction  $\alpha_R$ , as well as the on-site Cooper pairing  $\Delta$  are also staggered along the chain. The domain-wall, simulated by two adjacent stronger bonds, can host one JRBS (green cloud), while MF appears at the geometrical ends (red cloud). In the bottom model, s-wave superconducting pairing and antiferromagnetic (AF) order are introduced to a uniform semiconductor chain by the proximity effect. The domain-wall is simulated by an AF domain-wall. (b) A schematic illustration of the energy spectrum of bulk states, the eigen-energy of JRBS and MZES in the TSP. The blue regions represent the bulk band. The JRBS must continuously connect the particle and hole bands and inevitably go through zero energy at a point. The dotted line shows the eigen-energy of its antiparticle obeying the particle-hole symmetry.

pairing. The latter one is more easier to be carried out by sandwiching a semiconductor chain between an antiferromagnet (AF) and an ordinary s-wave superconductor. In our numerical calculation, the domain-wall is simulated by two adjacent stronger (weaker) bonds in the first model and by an AF domain-wall in the latter one. But our conclusions, in general, do not depend on the actual size and shape of the domain-walls.

*The first model.*—We start from a theoretical 1D Hamiltonian,

$$\begin{aligned}
 H = & \sum_{i\beta} \mu c_{i\beta}^\dagger c_{i\beta} + \sum_{i\beta\gamma} [1 - (-1)^i \delta] c_{i+1\beta}^\dagger \sigma_{\beta\gamma}^z c_{i\gamma} \\
 & + \sum_{i\beta\gamma} B c_{i\beta}^\dagger \sigma_{\beta\gamma}^z c_{i\gamma} + \alpha_R \sum_i (c_{i\uparrow}^\dagger c_{i+1\downarrow} - c_{i\downarrow}^\dagger c_{i+1\uparrow}) \\
 & + \sum_i \Delta c_{i\uparrow}^\dagger c_{i\downarrow}^\dagger + \text{h.c.}
 \end{aligned} \quad (1)$$

Here,  $c_{i\beta}$  and  $c_{i\beta}^\dagger$  are the annihilation and creation operators for spinful fermion with spin  $\beta$  on site  $i$  and  $\sigma$ 's are Pauli matrices. The energy units are set as the uniform part of hopping.  $\sigma^z$  appears in the hopping term because we have applied a transformation,  $c_{(2n+1)\downarrow} \rightarrow -c_{(2n+1)\downarrow}$ , on the odd sites of the lattice for the upper model showed in Fig. 1(a). The parameters  $\mu$ ,  $\delta$ ,  $\alpha_R$  and  $\Delta$  are for the strength of the chemical potential, the staggered part of hopping, the staggered spin-orbital interaction and the staggered superconducting pairing, respectively.

*The phase diagram of the first Hamiltonian.*— This model has two TSPs. The phase boundaries can be de-

termined by diagonalizing the Hamiltonian in the momentum space and figuring out the parameters at which the band gap closes. The detailed discussions are presented in the Supplemental Material [21]. We find that the two TSPs are in the parameter regions:  $\Delta^2 + \mu^2 + 4 - 4\sqrt{\Delta^2 + \mu^2} < B^2 < \Delta^2 + \mu^2 + 4 + 4\sqrt{\Delta^2 + \mu^2}$  (region II) and  $\Delta^2 + 4\delta^2 + \mu^2 - 4\alpha^2 - 4\sqrt{\Delta^2\delta^2 + \delta^2\mu^2 - \Delta^2\alpha^2} < B^2 < \Delta^2 + 4\delta^2 + \mu^2 - 4\alpha^2 + 4\sqrt{\Delta^2\delta^2 + \delta^2\mu^2 - \Delta^2\alpha^2}$  (region I), respectively. These regions will be explicitly indicated in Fig. 4. It should be noted that Region II is less dependent on  $\delta$  and can be regressed to the TSP of a uniform chain (without staggered hopping) when  $\delta = 0$ . But region I is a new TSP that appears only when  $|\delta| > |\alpha_R|$  with  $\mu = 0$ . It is only in this region that the FP JRBS emerges and the unavoidable zero energy crossing appears.

Next, we will use a topological argument to prove that each JRBS carries FP. From this, we can conclude that the zero energy crossing for JRBS is unavoidable. After that, the application of this property on controllable switching of the occupation states of a MZES is presented.

*Fractional parity JRBS.*— We use the evolution of Wannier functions (WF) during the Thouless pump to complete a topological proof of the assertion raised in the introduction.

We extend the Thouless pump (charge pump), first introduced to the spinless Su-Schrieffer-Heeger (SSH) model [12, 22–24], to the present spinful model. It is enrolled by modifying the Hamiltonian with an extra parameter  $\phi$ ,  $H(\phi) = H_0(\phi) + H_{\text{st}}(\phi)$ , where  $H_{\text{st}}(\phi) = \sum_i h_{\text{st}} \sin(\phi) (-1)^i (c_{i\uparrow}^\dagger c_{i\uparrow} - c_{i\downarrow}^\dagger c_{i\downarrow})$  and  $H_0(\phi)$  is the modified Hamiltonian by replacing  $\delta$  with  $\delta \cos(\phi)$  in Eq. 1. The absolute value of  $h_{\text{st}}$  is moderate so that the band gap at the Fermi energy is not closed during the pump.

The most localized WFs [25–27] for the occupied bands are obtained from the eigenvectors of the tilde position operator  $\tilde{R}(\phi) = \hat{P}(\phi) \hat{R} \hat{P}(\phi)$ , where  $\hat{R}$  is the position operator extended to the Nambu representation and  $\hat{P}(\phi) = \sum_{\alpha \in \text{occupied states}} |\alpha(\phi)\rangle \langle \alpha(\phi)|$  is the project operator on the occupied states ( $E < 0$ ) for the Hamiltonian  $H(\phi)$ . Here the position operator is  $\hat{R} = \text{diag}(1, 2, \dots, N) \tau_0$ , where  $\tau_0$  is the  $2 \times 2$  unit matrix in the particle-hole subspace and  $\text{diag}(1, 2, \dots, N)$  is a diagonal matrix with the diagonal elements running through lattice sites from 1 to  $N$ . The eigenvalues of  $\tilde{R}(\phi)$ , denoted as  $R_s$ , are the central positions of the WFs. It should be noticed that in the Nambu representation, each unit cell contributes 4 WFs while in a half filled spinless SSH model, it contributes only 1 WF.

In Fig. 2, we plot the energy spectrum (a) and the centers of WFs (b) during the Thouless pump with the parameters in region I. In this paper, only the positive eigenenergies are showed, while their symmetric negative counterparts are omitted. The energy spectrum shows

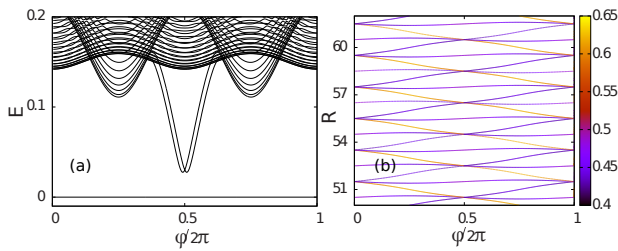


FIG. 2: The energy spectrum for  $H(\phi)$  with open boundary condition (a) and the associated centers of WFs (b). Only the positive eigenenergies are showed. The length of chain is  $N = 400$ . Parameters are  $\delta = 0.2$ ,  $\Delta = 0.3$ ,  $\mu = 0.1$ ,  $\alpha_R = 0.1$  and  $h_{st} = 0.3$ . The color palette in (b) is indicating the weights of WFs projected onto the particle subspace in Nambu representation.

that with the moderate value of  $h_{st} = 0.3$ , the band gap keeps open during the pump. This fact ensures that the WFs are localized and their centers showed in (b) are reliable. According to the evolution of centers of WFs showed in Fig. 2(b), these WFs can be classified into two groups, one corresponding to the WFs that do not change their position after a circle of pump and the other corresponding to the WFs that change their positions by one unit cell. The WFs in the latter group can be further divided into two kinds, one (in blue) is those moving in the positive direction with  $\phi$  and the other (in red) includes those moving inversely. In the Supplemental Material [21], we show that the Hamiltonian can be decoupled into two parts,  $H_{\pm}$ , when  $\mu = 0$ . Increasing  $\mu$  from 0 prohibits this decoupling but the topological properties of the band keep invariant until the gap closes. The above two groups of WFs inherit the evolution with  $\phi$  from those of the partial Hamiltonians  $H_{\pm}$ , respectively. The WFs inherited from those of  $H_{+}$  experience a trivial evolution (WFs come back to their initial positions) after a circle of pump while the other set that undergo a nontrivial evolution (WFs switch one unit cell) comes from those of  $H_{-}$ . If transforming  $H_{\pm}$  back to the lattice representation through an inverse Fourier transformation, one can find MF at the ends in  $H_{+}$  and JRBS at domain-wall in  $H_{-}$ .

We have also studied the evolution of WFs with the parameters in region II. But the WFs do not show any nontrivial evolution in that case.

Fig. 2(b) helps us to recognize that each JRBS carries FP. The topological proof includes 4 steps and we would like to highlight the goal of each step in the paper and put the details in the Supplemental Materials [21]. In the 1st step, besides the chains A and B raised in the introduction, an auxiliary chain C is employed. C is not uniform but with the pump parameter  $\phi$  varying slowly along it from 0 to  $2\pi$ . The other parameters are the same as those in the uniform chain A. From the evolution of WFs showed in Fig. 2 (b), on account of the total num-

bers of WFs, we can conclude that chains C and A are different by one pair of WFs. In the 2nd step, we prove that B and C have the same numbers of WFs. So with the bridge: chain C, we find that chain A and B are different by the pair of WFs. In the 3rd step, at a particular set of parameters,  $\mu = 0$ ,  $B = 0.3$  and  $\alpha_R = 0$ , the pair of WFs implies that the total number of quasi-particles in A and B are different by one in the representation of  $H_{\pm}$ . In the 4th step, after coming back to the original Nambu representation, the above one quasi-particle difference is equivalent to the parity difference between chains A and B. When the parameters leave away from these particular ones, the above conclusion is not modified as long as they are still in region I.

Through the above 4 steps, we have topologically proved that the total fermion parity on chains A and B,  $P_A$  and  $P_B$ , are different,  $|P_A - P_B| = 1$ . So each JRBS takes the responsibility of one half of the parity difference and FP comes out naturally. These conclusions can be confirmed numerically. We have numerically calculated the parity of the chains A and B with length  $N = 400$  and periodic boundary condition. The fermion parity is calculated by  $P = \text{rank}(v) \bmod 2$  [28], where  $\text{rank}(v)$  is the rank of Bogoliubov matrix  $v$ . We confirm that  $|P_A - P_B| = 1$  in region I and  $|P_A - P_B| = 0$  elsewhere.

*Electric charge carried by a JRBS.*— When the superconducting pairing is nonzero, JRBS abandons one of its most famous properties, fractional charge  $e/2$ , because the particle number is not well defined. We numerically confirm it by calculating the electric charge  $Q$  (in the units of  $e$ ) carried by a JRBS [24],

$$Q = \rho_L^{\text{WD}} - \rho_L^0, \quad (2)$$

where  $\rho_L^{\text{WD}}$  is the total particle number in a segment with a domain-wall at its center and  $\rho_L^0$  is the particle number for a segment without the domain-wall.  $L$  is the length of these segments which should exceed the localization length of JRBS. In the numerical calculation, we choose  $L = 200$  which is long enough for a saturated  $Q$ .

The calculated  $Q$  as a function of  $B$  is showed in Fig. 3. It is confirmed that the electric charge  $Q$  becomes non-universal and is dependent on  $\mu$ , as well as on  $B$  in region I. When  $\mu = 0$ , the domain-wall becomes neutral because the particle number on each site is exactly one, independent of the presence of domain-wall. When  $\mu \neq 0$ , the nonzero  $Q$  is smoothly varying in region I, except near  $B_0$  at which its sign is switched. This sign switching is directly associated with the zero energy crossing for JRBS showed in the inset. In inset, we show the energy spectrum for the ring with  $\mu = 0.4$ . The eigen-energy inside the bulk gap is for the JRBS on domain-wall. It is the particle-hole transition for the JRBS around the zero energy crossing point that changes the sign of electrical charge  $Q$ .

In region II, the charge shows a peak and a dip at the phase boundaries. But it is almost zero inside the region.

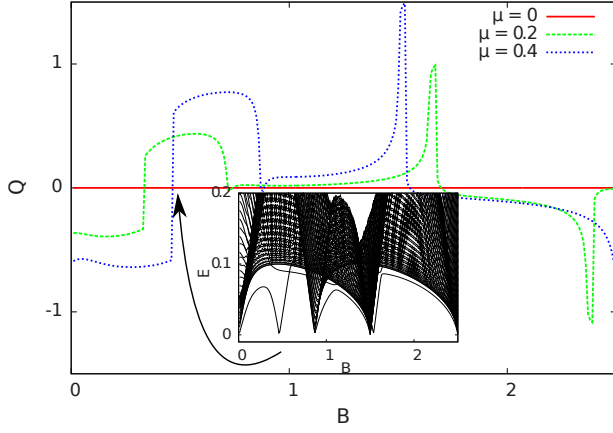


FIG. 3: (Color online) Electric charge carried by a domain-wall. The system is a ring embedded with a domain-wall with the parameters,  $\delta = 0.2$ ,  $\Delta = 0.3$  and  $\alpha_R = 0.1$ . The length of the ring is  $N = 401$  and the length of the segments are  $L = 200$ .  $\rho_L^{\text{WD}}$  and  $\rho_L^0$  are numerically calculated on a half of the ring with the domain-wall at the center and on the part of the rest half, respectively. The inset shows the energy spectrum for the ring with  $\mu = 0.4$ . The arrow indicates the consistence of the point at where the zero energy crossing happens and electric charge  $Q$  switches sign.

We suggest that the peak and dip are due to the quantum fluctuation accompanied with the band gap closing.

*Unavoidable zero energy crossing.*— The energy spectrum in inset of Fig. 3 shows a zero energy crossing for JRBS. Now we apply a topological argument to prove that the zero energy crossing is unavoidable. We start from a proof by contradiction by supposing that the energy spectrum for JRBS does not cross zero energy. One can modify the factors, i.e., the size of the domain-wall, so that its eigen-energy is near the bulk band but not deeply inside the band gap. In this case, the eigen-energy of JRBS is not different from that of a normal impurity. When embedding such a domain-wall in a uniform chain, the contribution of fermion parity from it is fixed, either 0 or 1. When the embedded domain-walls become two, the total contributions of fermion parity from them become 0. But as we have showed,  $|P_A - P_B| = 1$ , which requires that the two JRBSs must contribute an extra fermion parity 1. Here, we get contradicting results and the initial assumption must be wrong. So the FP JRBS in TSP in region I must trigger an eigen-state with its eigen-energy crossing the zero energy inevitably. In the Supplemental Materials[21], we have confirmed numerically that the zero energy crossing is robust against a strong lattice distortion.

*Majorana Fermion and JRBS.*— In the previous discussion, our focus is on JRBS. In this section, we show the coexistence of MF and JRBS and how to switch between the empty state and the occupied state of MZES with the help of JRBS.

In Fig. 4, we show the typical energy spectrum for an

open chain embedded with a domain-wall at the center. In region I, the persistent zero energy state is MZES and the nonzero eigen-energy of JRBS crosses the zero energy at  $B_0$ . As showed explicitly in the figure, the wave-functions of these states are localized at the domain-wall for JRBS and at the geometrical ends for MZES.

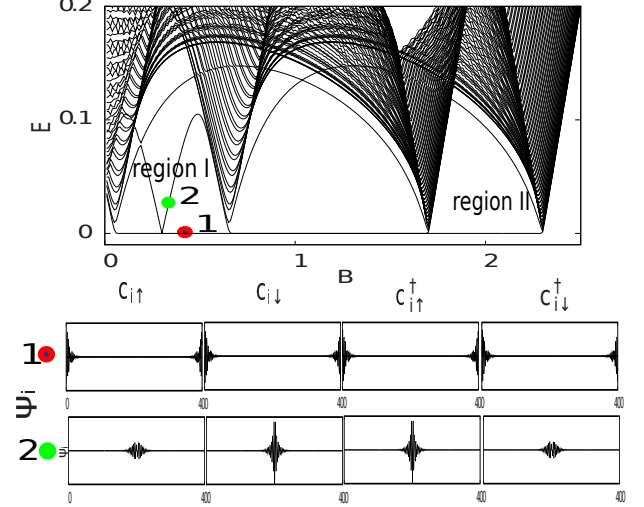


FIG. 4: (Color online) Upper panel: energy spectrum for the chain embedded with a domain-wall. Lower panel: amplitudes of wavefunctions of MZES and JRBS in representation  $(c_{i\uparrow}, c_{i\downarrow}, c_{i\uparrow}^\dagger, c_{i\downarrow}^\dagger)^T$ , where  $i$  runs through the lattice sites from 1 to  $N = 401$ . The other parameters are the same as those in Fig. 3 except  $\mu = 0$ .

When we ignore the MZES by modifying the geometry of the model from chain to ring (no geometrical ends). It is known that the fermion parity of ground state of the ring is changed when  $B$  is varying across  $B_0$  because of the zero energy crossing. This is confirmed by the numerical calculation on the parity of the ring. So the ground states on  $B < B_0$  and  $B > B_0$  in region I have different fermion parity. Therefore, if we increase  $B$  to cross  $B_0$  with a ring at its ground state initially, the final state must be an excited state and can not spontaneously jump back to the final ground state because the parity is conserved in this process.

When the MZES is reconsidered in a chain, the above excited state can jump back to the final ground state by a parity compensation on MZES. This compensation is achieved by the switching between the empty state and the occupied state of MZES because this switching contributes one parity change. In this manner, with the help of a JRBS embedded in the chain, we would be able to flip between the two states of the MZES still in the restriction that the total fermion parity is conserved. A quantum qubit can be encoded into these two states of one MZES, while in chains without JRBS, two MZESs are needed.

*The second model with local AF order.*— The second model is schematically showed at the bottom of Fig. 1(a).

It is the AF order that doubles the unit cell.

We find that this model also possesses two TSPs[21]. In one of these TSPs, called as region I, JRBS bounded on an AF domain-wall can also coexists with MZES. Through a parity calculation on the rings A and B in this new model, we confirm that the JRBS also carries FP. As we have discussed in the previous model, this means that the eigen-energy of JRBS must suffer an unavoidable zero energy crossing in region I. A detailed discussion is presented in the Supplemental Material [21].

*Conclusions.*— We have showed that JRBS and MF can coexist in a TSP in 1D models. The eigen-energy of the FP JRBS suffers an unavoidable zero energy crossing. This crossing separates the TSP into two parts with different parities for the ground state. This can be used to switch between the occupied and the empty states of MZES under the conservation of total fermion parity. One should be able to observe such effect by measuring the Josephson current through MZES. As the magnetic field is modified across the crossing point, the Josephson current should suffer a sudden sign jump because the parity on the MZES is changed. It still remains challenging how to experimentally observe the FP JRBS directly. One possible way is to apply the proposal in Ref. [19], although the electric charge on the domain-wall is not  $e/2$  in this case.

*Acknowledgments.*— The work was supported by the State Key Program for Basic Research of China (Grant Nos. 2009CB929504, 2009CB929501), National Foundation of Natural Science in China Grant Nos. 10704040, 11175087.

---

\* Electronic address: xiongye@njnu.edu.cn

† Electronic address: pqotong@njnu.edu.cn

- [1] D. a. Ivanov, Phys. Rev. Lett. **86**, 268 (2001), ISSN 0031-9007.
- [2] X.-L. Qi and S.-C. Zhang, Rev. Mod. Phys. **83**, 1057 (2011).
- [3] C. Nayak, S. H. Simon, A. Stern, M. Freedman, and S. Das Sarma, Rev. Mod. Phys. **80**, 1083 (2008).
- [4] X.-J. Liu, T. Law, K., and K. Ng, T., Phys. Rev. Lett. **112**, 086401 (2014).
- [5] L. Fu and C. L. Kane, Phys. Rev. Lett. **100**, 096407 (2008).
- [6] X.-L. Qi, T. L. Hughes, and S.-C. Zhang, Phys. Rev. B **82**, 184516 (2010).
- [7] X.-W. Yan, M. Gao, Z.-Y. Lu, and T. Xiang, Phys. Rev. B **84**, 054502 (2011).
- [8] Y. Tanaka, M. Sato, and N. Nagaosa, Journal of the Physical Society of Japan **81**, 011013 (2012).
- [9] J. J. He, K. Ng, T., P. A. Lee, and T. Law, K., Phys. Rev. Lett. **112**, 037001 (2014).
- [10] A. Y. Kitaev, Phys. Usp. **44**, 131 (2001).
- [11] J. D. Sau, R. M. Lutchyn, S. Tewari, and S. Das Sarma, Phys. Rev. Lett. **104**, 040502 (2010).
- [12] S.-Q. Shen, *Topological Insulators, Dirac Equation in Condensed Matters* (Springer Series in Solid-State Science 174, 2012).
- [13] J. Klinovaja, P. Stano, and D. Loss, Phys. Rev. Lett. **109**, 236801 (2012).
- [14] A. C. Potter and P. A. Lee, Phys. Rev. Lett. **105**, 227003 (2010).
- [15] R. Wakatsuki, M. Ezawa, Y. Tanaka, and N. Nagaosa, Phys. Rev. B **90**, 014505 (2014).
- [16] M. Z. Hasan and C. L. Kane, Rev. Mod. Phys. **82**, 3045 (2010).
- [17] R. Jackiw and C. Rebbi, Phys. Rev. D **13**, 3398 (1976).
- [18] S. Gangadharaiah, L. Trifunovic, and D. Loss, Phys. Rev. Lett. **108**, 136803 (2012).
- [19] D. Rainis, A. Saha, J. Klinovaja, L. Trifunovic, and D. Loss, Phys. Rev. Lett. **112**, 196803 (2014).
- [20] J. I. Väyrynen and T. Ojanen, Phys. Rev. Lett. **107**, 166804 (2011).
- [21] See Supplemental Material for the detailed phase diagram of the first model, the topological argument on fractional parity and the detailed discussion about the second model.
- [22] W. P. Su, J. R. Schrieffer, and A. J. Heeger, Phys. Rev. Lett. **42**, 1698 (1979).
- [23] W. P. Su, J. R. Schrieffer, and A. J. Heeger, Phys. Rev. B **22**, 2099 (1980).
- [24] S. Kivelson and J. R. Schrieffer, Phys. Rev. B **25**, 6447 (1982).
- [25] D. Thouless, J. Phys. C **17**, L325 (1984).
- [26] T. Thonhauser and D. Vanderbilt, Phys. Rev. B **74**, 235111 (2006).
- [27] X.-L. Qi, Phys. Rev. Lett. **107**, 126803 (2011).
- [28] G. Ben-Shach, A. Haim, I. Appelbaum, Y. Oreg, A. Yacoby, and B. I. Halperin, arXiv:1406:5172.

# Supplemental material for: Jackiw-Rebbi-type bound state carrying fractional parity

Ye Xiong

*Department of Physics and Institute of Theoretical Physics ,  
Nanjing Normal University, Nanjing 210023, P. R. China*

Peiqing Tong

*Department of Physics and Institute of Theoretical Physics ,  
Nanjing Normal University, Nanjing 210046, P. R. China  
Jiangsu Key Laboratory for Numerical Simulation of Large Scale Complex Systems,  
Nanjing Normal University, Nanjing 210023, P. R. China and  
Kavli Institute for Theoretical Physics China, CAS, Beijing 100190, China*

PACS numbers: 73.63.Nm, 74.45.+c, 14.80.Va, 75.60.Ch

## I. THE FIRST HAMILTONIAN.

We are considering cold fermions trapped in a 1D laser induced lattice. The staggered hoppings like that in the SSH model has been realized in the experiment<sup>1,2</sup>. In a recent proposal<sup>3</sup>, the staggered effective spin-orbital interaction can also be produced with the aid of modern technologies. It was also known that 1D Fermi gas with spin orbital coupling was dominated by Fulde-Ferrell (FF) superfluid phase at low temperature<sup>4-7</sup>. In this paper, we simulate the FF phase with a stagger pairing coefficient. So the Hamiltonian reads

$$H = \sum_{i\beta} \mu c_{i\beta}^\dagger c_{i\beta} + \sum_{i\beta} [1 - (-1)^i \delta] c_{i\beta}^\dagger c_{i+1\beta} + \sum_{i\beta\gamma} B c_{i\beta}^\dagger \sigma_{\beta\gamma}^z c_{i\gamma} - \sum_i (-1)^i \alpha_R (c_{i\uparrow}^\dagger c_{i+1\downarrow} + c_{i\downarrow}^\dagger c_{i+1\uparrow}) + \sum_i (-1)^i \Delta c_{i\uparrow}^\dagger c_{i\downarrow}^\dagger + \text{h.c.}, \quad (1)$$

where chemical potential, staggered hoppings, magnetic field induced Zeeman term, staggered spin-orbital interaction and FF superfluid pairing are written, subsequently.  $\sigma$ 's are Pauli matrices and  $c_{i\beta}$  is annihilation operator on site  $i$  with spin  $\beta$ . Through a transformation on the odd lattice,  $c_{2n+1\uparrow} \rightarrow c_{2n+1\uparrow}$  and  $c_{2n+1\downarrow} \rightarrow -c_{2n+1\downarrow}$ , the staggered spin-orbital and superconducting interactions are smeared out in the new representation and the Hamiltonian changes to

$$H = \sum_{i\beta} \mu c_{i\beta}^\dagger c_{i\beta} + \sum_{i\beta\gamma} [1 - (-1)^i \delta] c_{i+1\beta}^\dagger \sigma_{\beta\gamma}^z c_{i\gamma} + \sum_{i\beta\gamma} B c_{i\beta}^\dagger \sigma_{\beta\gamma}^z c_{i\gamma} + \sum_i \alpha_R (c_{i\uparrow}^\dagger c_{i+1\downarrow} - c_{i\downarrow}^\dagger c_{i+1\uparrow}) + \sum_i \Delta c_{i\uparrow}^\dagger c_{i\downarrow}^\dagger + \text{h.c.}, \quad (2)$$

which is the first Hamiltonian we studied in the letter.

### A. The phase diagram of the first model.

We study the model with periodic boundary condition so that the wave vector  $k$  is a good quantum number. A unit cell includes two sub-lattices denoted by  $A$  and  $B$  respectively. The Hamiltonian in the Hilbert space  $(\psi_{kA\uparrow}, \psi_{kB\uparrow}, \psi_{kA\downarrow}, \psi_{kB\downarrow}, \psi_{-kA\uparrow}^\dagger, \psi_{-kB\uparrow}^\dagger, \psi_{-kA\downarrow}^\dagger, \psi_{-kB\downarrow}^\dagger)^T$  reads

$$H(k) = \begin{pmatrix} H_0(k) & V(k) \\ V^\dagger(k) & -H_0(k) \end{pmatrix}, \quad (3)$$



where

$$H_0(k) = \begin{pmatrix} B + \mu & (1 + \delta) + (1 - \delta)e^{-ik} & 0 & \alpha_R(1 - e^{-ik}) \\ (1 + \delta) + (1 - \delta)e^{ik} & B + \mu & -\alpha_R(1 - e^{ik}) & 0 \\ 0 & -\alpha_R(1 - e^{-ik}) & -B + \mu & -[(1 + \delta) + (1 - \delta)e^{-ik}] \\ \alpha_R(1 - e^{ik}) & 0 & -[(1 + \delta) + (1 - \delta)e^{ik}] & -B + \mu \end{pmatrix}$$

and

$$V(k) = \begin{pmatrix} 0 & 0 & \Delta & 0 \\ 0 & 0 & 0 & \Delta \\ -\Delta & 0 & 0 & 0 \\ 0 & -\Delta & 0 & 0 \end{pmatrix}.$$

Through a unitary transformation

$$U = \frac{1}{\sqrt{2}} \begin{pmatrix} I & I \\ I & -I \end{pmatrix},$$

the Hamiltonian is transformed to

$$H(k) \rightarrow UH(k)U^{-1} = \begin{pmatrix} 0 & A(k) \\ A^\dagger(k) & 0 \end{pmatrix},$$

where  $I$  is a  $4 \times 4$  unit matrix and  $A(k) = H_0(k) + V(k)$ .

For a gapped ring, the gap should close at  $k = 0$  or  $k = \pi$  in the Brillouin zone as varying parameters. At these phase boundaries, the nonzero bulk wavefunction at  $E = 0$  implies  $\det(A) = 0$ . So we have the two phase boundary conditions,  $B^2 = \Delta^2 + \mu^2 + 4 \pm 4\sqrt{\Delta^2 + \mu^2}$  from  $k = 0$  and  $B^2 = \Delta^2 + 4\delta^2 + \mu^2 - 4\alpha^2 \pm 4\sqrt{\Delta^2\delta^2 + \delta^2\mu^2 - \Delta^2\alpha^2}$  from  $k = \pi$ .

In Fig. 1, we sketch the phase diagram in  $B - \mu$ ,  $B - \alpha$ ,  $B - \Delta$  and  $B - \delta$  planes, respectively by numerically diagonalizing  $H(k)$ . The phase boundaries are consistent with the above two conditions except on the  $B$  axis when  $\alpha = 0$  or  $\Delta = 0$ . This deviation is because in these particular conditions, the model is gapless, which violates our assumption that the gap closes at  $k = 0$  or  $k = \pi$ .

A topological invariant can be defined by  $M = \frac{\Phi_{ZB}}{\pi} \bmod 2$ , where  $\Phi_{ZB}$  is the Zak-Berry phase integrated over the whole Brillouin zone  $\Phi_{ZB} = \int_{-\pi}^{\pi} -i\langle\psi|\partial_k|\psi\rangle dk$  and  $|\psi\rangle$  are the occupied band states. The above topological invariant specified by Zak-Berry phase is equivalent to the Pfaffian invariant first introduced by Kitaev in studying 1D topological



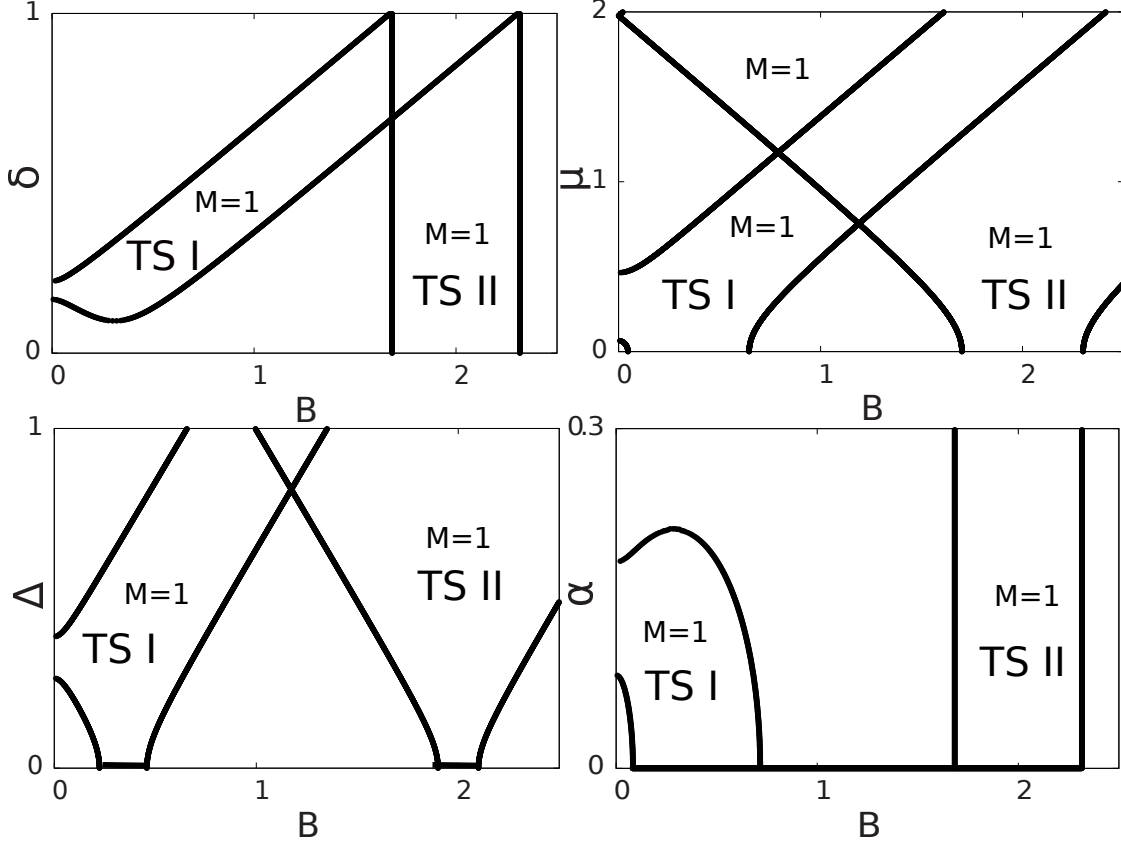


FIG. 1: The phase diagram in  $B - \delta$  (a) ,  $B - \mu$  (b),  $B - \Delta$  (c) and  $B - \alpha_R$  (d) planes. The other parameters are  $\mu = 0.1$ ,  $\alpha_R = 0.1$  and  $\Delta = 0.3$  in (a),  $\alpha_R = 0.1$ ,  $\Delta = 0.3$  and  $\delta = 0.2$  in (b),  $\alpha_R = 0.1$ ,  $\delta = 0.2$  and  $\mu = 0.1$  in (c) and  $\delta = 0.2$ ,  $\mu = 0.1$  and  $\Delta = 0.3$  in (d). The regions in the TSP with a topological invariant  $M = 1$  have been indicated explicitly. The rest regions are for topological trivial phase with  $M = 0$ . The coexistence of MF and JRBS happens only in the TPS indicated by “TS I”.

superconductor<sup>8</sup>. In Fig. 1, we indicate the regions in topological superconducting phase (TSP) with  $M = 1$ . The rest regions are for topological trivial phase with  $M = 0$ . Among these topological nontrivial regions, MFs and JRBS can only coexist in region I which is a new region stemming from staggered hopping but not in region II stemming from  $B = 2$ .

These topological nontrivial phases can be confirmed by the existence of boundary states at the geometrical ends. In Fig. 2(a), we plot energy spectrum for the Hamiltonian with open boundary condition. The length of the chain is  $N = 400$  and the chemical potential is  $\mu = 0$ . There is one Majorana zero energy state (MZES) in the band gap in two regions: region I in  $0.05 < |B| < 0.65$  and region II in  $1.7 < |B| < 2.3$ . There is also another exotic

region in  $0.65 < |B| < 1.7$ , where two MZESs appear. The double-degenerate Kramers MF bound states have been discussed in a two-chains model with particle-hole and time-reversal symmetry in Ref.<sup>9,10</sup>. The two zero-energy bound states in our model are similar to this MF pair but the time-reversal symmetry has been replaced by the sublattice symmetry when  $\mu = 0$ .

In Fig. 2(b), we plot the energy spectrum for the model with periodic boundary condition and the length of ring is changed to  $N = 401$ . As the length of the unit cell is 2, the ring contains insuppressible half unit cell. So this ring naturally engages a domain-wall and the energy spectrum exhibits bound states near it. In Fig. 2(b) MZES disappears as there is no geometric end. Outside region I, the energies of bound states are adjacent to the bulk band, implying that the domain-wall can only be considered as a normal impurity. In region I, however, a bound state deep in gap can evolve continuously crossing the zero energy. This implies that domain-wall in region I should be considered as a topological impurity that triggers *one* JRBS.

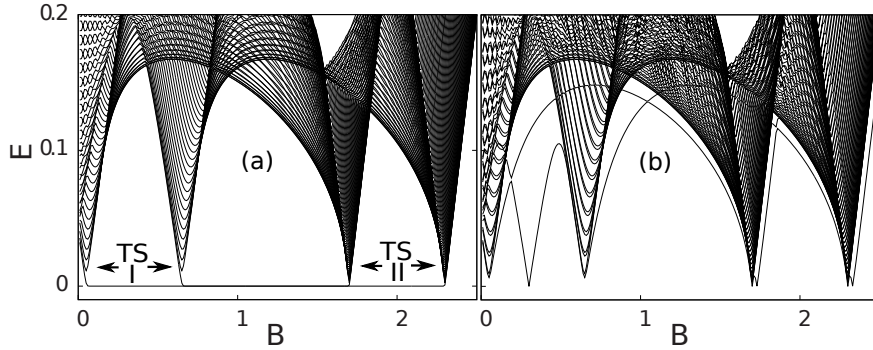


FIG. 2: The energy spectrum for  $N = 400$  chain with open boundary condition (a) and for  $N = 401$  ring with periodic boundary condition (b). Parameters are  $\delta = 0.2$ ,  $\Delta = 0.3$ ,  $\alpha_R = 0.1$  and  $\mu = 0$ . In (a), a single MZES appears in two regions: region I  $0.05 < |B| < 0.65$  and region II  $1.7 < |B| < 2.3$ . There are two MZESs in the region  $0.65 < |B| < 1.7$ . Panel (b) shows that a domain-wall can bring *one* bound state deep in band gap in region I.

### B. Another way to understand TSP when $\mu = 0$ .

When  $\mu = 0$ , through a unitary transformation

$$U = \frac{1}{\sqrt{2}} \begin{pmatrix} 1 & 0 & 0 & 0 & 0 & 0 & -1 & 0 \\ 0 & 1 & 0 & 0 & 0 & 0 & 0 & -1 \\ 0 & 0 & 1 & 0 & -1 & 0 & 0 & 0 \\ 0 & 0 & 0 & 1 & 0 & -1 & 0 & 0 \\ 0 & 0 & 1 & 0 & 1 & 0 & 0 & 0 \\ 0 & 0 & 0 & 1 & 0 & 1 & 0 & 0 \\ 1 & 0 & 0 & 0 & 0 & 0 & 1 & 0 \\ 0 & 1 & 0 & 0 & 0 & 0 & 0 & 1 \end{pmatrix},$$

the Hamiltonian can be decoupled into two partitioning parts

$$H \rightarrow U H U^\dagger = \begin{pmatrix} H_+ & 0 \\ 0 & H_- \end{pmatrix}, \quad (4)$$

where

$$H_- = - \begin{pmatrix} B - \Delta & (1 + \delta) + (1 - \delta)e^{-ik} & 0 & \alpha_R(1 - e^{-ik}) \\ (1 + \delta) + (1 - \delta)e^{ik} & B - \Delta & -\alpha_R(1 - e^{ik}) & 0 \\ 0 & -\alpha_R(1 - e^{-ik}) & -B + \Delta & -[(1 + \delta) + (1 - \delta)e^{-ik}] \\ \alpha_R(1 - e^{ik}) & 0 & -[(1 + \delta) + (1 - \delta)e^{ik}] & -B + \Delta \end{pmatrix}$$

and

$$H_+ = \begin{pmatrix} B + \Delta & (1 + \delta) + (1 - \delta)e^{-ik} & 0 & \alpha_R(1 - e^{-ik}) \\ (1 + \delta) + (1 - \delta)e^{ik} & B + \Delta & -\alpha_R(1 - e^{ik}) & 0 \\ 0 & -\alpha_R(1 - e^{-ik}) & -B - \Delta & -[(1 + \delta) + (1 - \delta)e^{-ik}] \\ \alpha_R(1 - e^{ik}) & 0 & -[(1 + \delta) + (1 - \delta)e^{ik}] & -B - \Delta \end{pmatrix}.$$

We show the dispersion of the eigen-energies for the two partitioning parts,  $H_-$  and  $H_+$ , in different phases in Fig. 3, respectively. (a), (c), (e) and (g) are for  $H_-$  and (b), (d), (f), (h) are for  $H_+$ . The four rows of panels show the dispersion with  $B = 0.3$  (in region I),  $B = 1$ ,  $B = 2$  (in region II) and  $B = 2.6$ , respectively. The band inversion happens only in one part of the Hamiltonian in regions I and II. This is consistent with our conclusions in the letter that region I and II are in TSP with only one MZES. The region in between I and II can host totally two MZESs, one in  $H_+$  and the other in  $H_-$ .

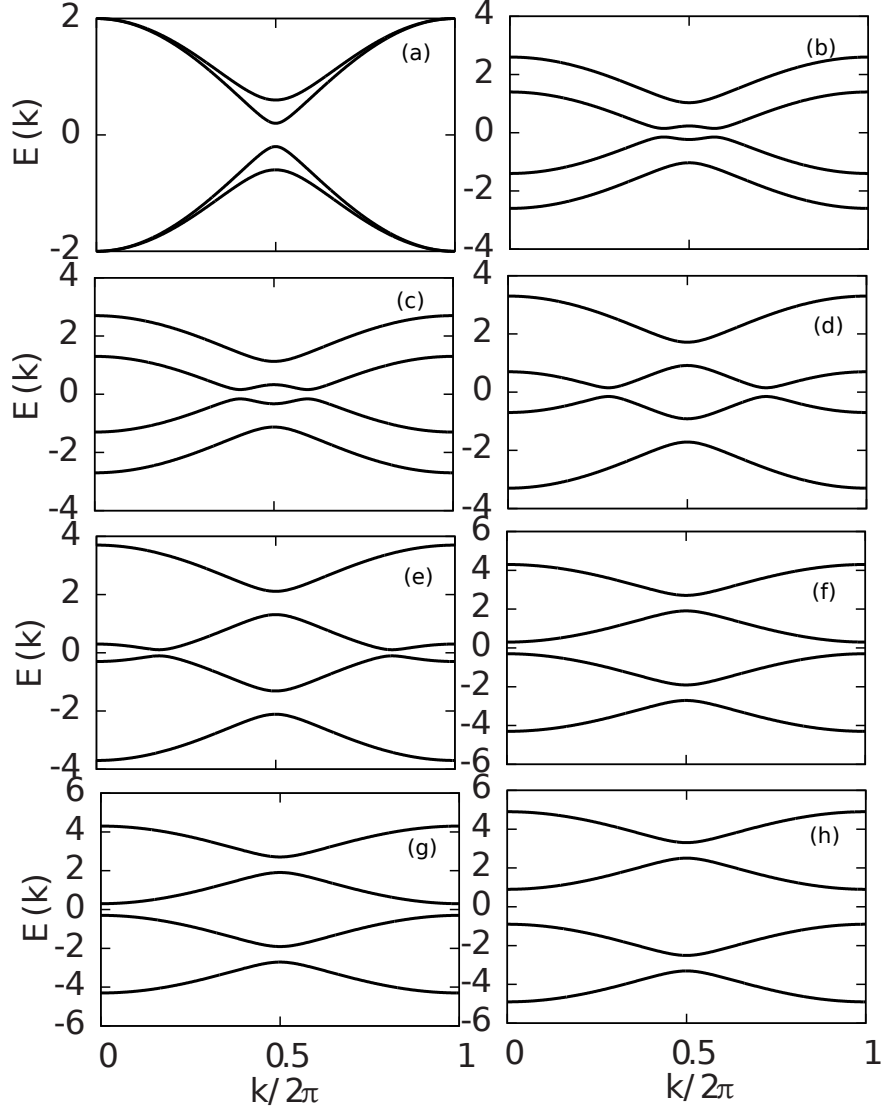


FIG. 3: The band dispersion with  $k$  for the two partial Hamiltonians,  $H_-$  (a) (c) (e) (g) and  $H_+$  (b) (d) (f) (h). The parameters are  $\alpha_R = 0.1$ ,  $\delta = 0.2$ ,  $\Delta = 0.3$  and  $B = 0.3$  (a) (b),  $B = 1$  (c) (d)  $B = 2$  (e) (f) and  $B = 2.6$  (g) (h).

### C. The evolution of the centers of Wannier functions during Thouless pump for the two partial Hamiltonians.

In Fig. 4, we plot the evolution of the centers of Wannier functions during Thouless pump for the two partial Hamiltonians,  $H_+$  and  $H_-$ , respectively. If we combine the two panels together, we reproduce Fig. 2 (b) in the paper.

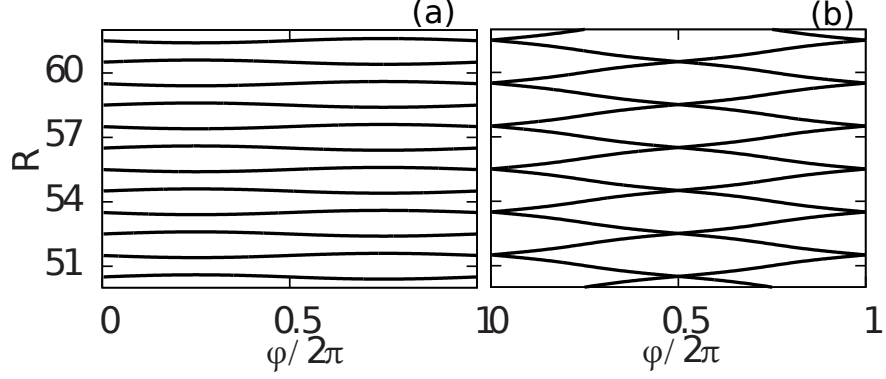


FIG. 4: The evolution of the centers of Wannier functions during Thouless pump for the two partial Hamiltonians,  $H_+$  (a) and  $H_-$  (b). The parameters are same as those in Fig. 2 in the paper except  $\mu = 0$ .

#### D. Fractional parity JRBS, a topological proof.

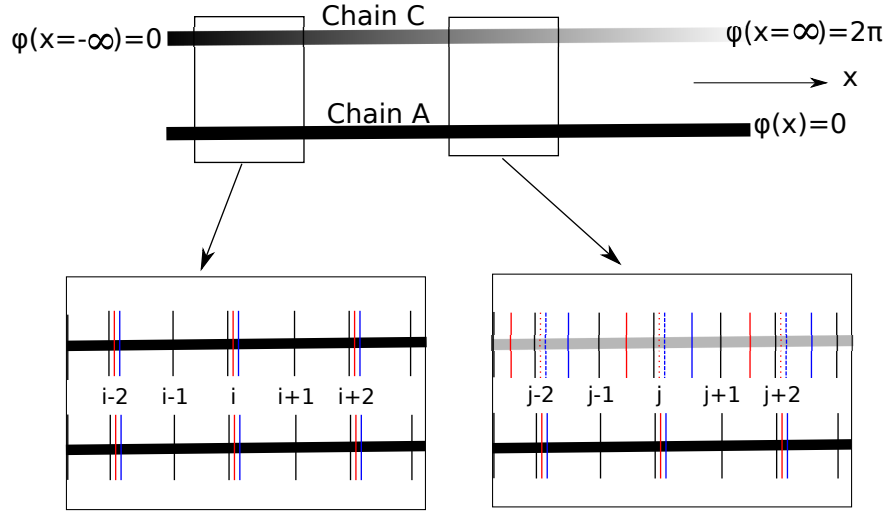


FIG. 5: Chain C is describing by the extended Thouless pump Hamiltonian  $H(\phi(x))$  with  $\phi(x)$  slowly varying along the chain. The short vertical lines in the two zoomed pictures represent the localized WFs. There are 4 WFs in each unit cell and  $i, j$  are used to denote the positions along the chain.

*The first step.*— Let us compare the positions of WFs in two infinite chains A and C, which are described by the Thouless pump Hamiltonian  $H(\phi)$ . Chain A is a uniform chain with  $\phi = 0$  (the Hamiltonian regresses to Eq. 1 in the paper) and B is a chain on which  $\phi$  is slowly varying  $2\pi$  along it, which have been schematically showed in Fig. 5. Without

loss of generality, we let  $\phi(x = -\infty) = 0$  and  $\phi(x = \infty) = 2\pi$  in C. Because  $\phi(x)$  is varying very slowly, in each macroscopically small but microscopically large segments, it can be considered as a constant. This ensures us to find the positions of the WFs in each segment in the latter chain. For the segments at  $x = -\infty$ , the positions of WFs in two chains are identical. But as  $x$  is increasing, compared with those in A, a set of WFs (in blue) in C begins to misalign slightly in the positive  $x$  direction while another set of WFs (in red) has misaligned simultaneously in the negative direction, as showed in the figure. These WFs in blue or red have been showed in Fig. 2 in the paper. As we sweeping our focus through the chains from  $x = -\infty$  to  $x = +\infty$ , the above misalignments increase and finally reach  $\pm 2$ , the length of a unit cell. This can be considered as that turning on  $\phi(x)$  will push a WF (in blue) outside and pull a WF (in red) in at  $x = +\infty$ . So we can conclude that compared with the uniform chain, C donates one WF (in blue) and accepts another WF (in red).

*The second step.*— Now we relax the restriction that  $\phi(x)$  is varying slowly along C. This relaxation does not affect the above conclusion because local fluctuations of  $\phi(x)$  can not distort the global property happening at  $x = +\infty$ . For simplicity, we let  $\phi(x)$  jumps  $\pi$  at two long separate points and keeps constant elsewhere. This new layout of  $\phi(x)$  is just describing a chain with a pair of domain-walls, which is chain B actually. So this pair of domain-walls must take the responsibility of the pair of WFs that have been lost and gained. Because the two domain-walls are identical through a mirror reflection, their properties must be the same. So each domain-wall is in response to *one half* of the WF pair.

*The third step.*— With the particular parameters,  $\mu = 0$ ,  $\delta = 0.2$ ,  $\Delta = 0.3$ ,  $B = 0.3$  and  $\alpha_R = 0$ , the Hamiltonian  $H(k)$  can be decoupled into two parts,  $H_{\pm}$ . The pair of WFs that have been lost and gained comes from those of  $H_-$ . So we only need to focus on the partial Hamiltonian  $H_-$ , which has been given explicitly. In this representation,  $\alpha_R$  is playing the role of superconducting pairing in this partner Hamiltonian. When  $\alpha_R = 0$ , this Hamiltonian regresses to a standard spinless SSH model. The dimension of  $H_-$  has been extended from that of the standard spinless SSH model,  $2 \times 2$ , to  $4 \times 4$  because a Nambu representation is still taken. The two sets of WFs, in blue and in red, come from the empty conduction band and the filled valence band of the SSH model, respectively<sup>11</sup>. So in the representation of  $H_-$ , the pair of lost and gained WFs corresponds to one quasi-particle difference.

*The fourth step.*— After returning back to the ordinal Nambu representation of  $H(k)$ , the one quasi-particle difference between A and B corresponds to the difference of the parities of

fermion numbers in A and B. Tuning on  $\alpha_R$  and  $\mu$  does not disturb this conclusion because the spin-orbital interaction and chemical potential commute with particle number operator so that they also commute with the parity. As each JRBS takes the responsibility of half of this parity difference, we conclude that it carries FP in the presence of superconducting pairing.

#### E. The robust zero energy crossing against disorder.

We distort the perfect lattice in Fig. 4 in the paper by the disorder,  $\delta_i = \delta(1 + w_i)$ , where  $\delta = 0.2$  and  $w_i$  randomly distributes in  $[-0.6, 0.6]$ . The spectrum is showed in Fig. 6. It shows that the zero energy crossing for the eigen-energy of JRBS is robust against the lattice distortion.

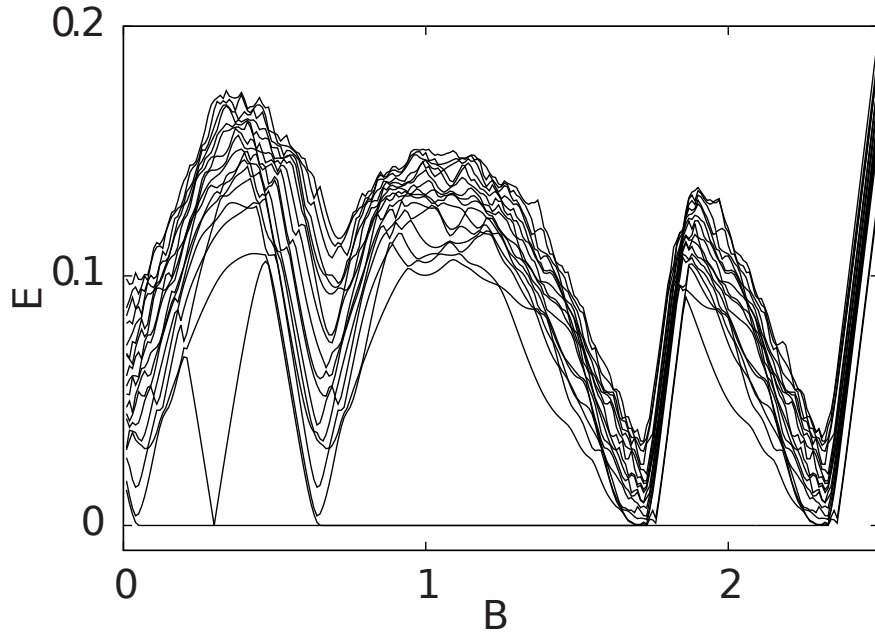


FIG. 6: The energy spectrum for a disordered lattice. The eigen-energy of JRBS can still cross the zero energy.



## II. THE SECOND MODEL WITH LOCAL AF ORDER.

The Hamiltonian reads,

$$\begin{aligned}
H = & \sum_{i\beta} [c_{i\beta}^\dagger c_{i+1\beta} + \mu c_{i\beta}^\dagger c_{i\beta}] + i\alpha_R \sum_{i\beta\gamma} c_{i\beta}^\dagger \sigma_{\beta\gamma}^y c_{i+1\gamma} \\
& + \sum_{i\beta\gamma} c_{i\beta}^\dagger (\vec{B} - \vec{M}_i) \cdot \vec{\sigma}_{\beta\gamma} c_{i\gamma} + \sum_i \Delta c_{i\uparrow}^\dagger c_{i\downarrow}^\dagger + \text{h.c.},
\end{aligned} \tag{5}$$

where hopping, chemical potential, spin-orbital interaction, Zeeman interaction caused by a uniform magnetic field  $\vec{B}$  and staggered local magnetic momenta  $\vec{M}_i$  and s-wave superconducting pairing are expressed, respectively. We fix the magnetic field in the  $x - z$  plane with  $\vec{B} = \sin(\theta)B\hat{z} + \cos(\theta)B\hat{x}$  and the staggered local AF momenta are in the  $x$  direction,  $\vec{M}_i = (-1)^i M\hat{x}$ . In experiment, AF magnetic order and s-wave superconducting pairing can be introduced to a 1D semi-conductor through proximity effect by sandwiching it with AF material and superconductor.

This Hamiltonian in the Hilbert space  $(\psi_{kA\uparrow}, \psi_{kB\uparrow}, \psi_{kA\downarrow}, \psi_{kB\downarrow}, \psi_{-kA\uparrow}^\dagger, \psi_{-kB\uparrow}^\dagger, \psi_{-kA\downarrow}^\dagger, \psi_{-kB\downarrow}^\dagger)^T$  reads

$$H = \begin{pmatrix} H_0 & V \\ V^\dagger & -H_0 \end{pmatrix}, \tag{6}$$

where

$$H_0 = \begin{pmatrix} \mu + B \sin(\theta) & 1 + e^{-ik} & B \cos(\theta) + M & \alpha_R(1 - e^{-ik}) \\ 1 + e^{ik} & \mu + B \sin(\theta) & -\alpha_R(1 - e^{ik}) & B \cos(\theta) - M \\ B \cos(\theta) + M & -\alpha_R(1 - e^{-ik}) & \mu - B \sin(\theta) & 1 + e^{-ik} \\ \alpha_R(1 - e^{ik}) & B \cos(\theta) - M & 1 + e^{ik} & \mu - B \sin(\theta) \end{pmatrix},$$

and

$$V = \begin{pmatrix} 0 & 0 & \Delta & 0 \\ 0 & 0 & 0 & \Delta \\ -\Delta & 0 & 0 & 0 \\ 0 & -\Delta & 0 & 0 \end{pmatrix}.$$

When  $\mu = 0$ , the above Hamiltonian can also be decoupled into two partitioning parts,

$$H \rightarrow \begin{pmatrix} H_+ & 0 \\ 0 & H_- \end{pmatrix}, \tag{7}$$

where

$$H_+ = \begin{pmatrix} B \sin(\theta) + \Delta & 1 + e^{-ik} & B \cos(\theta) + M & \alpha_R(1 - e^{-ik}) \\ 1 + e^{ik} & B \sin(\theta) - \Delta & -\alpha_R(1 - e^{ik}) & B \cos(\theta) - M \\ B \cos(\theta) + M & -\alpha_R(1 - e^{-ik}) & \Delta - B \sin(\theta) & 1 + e^{-ik} \\ \alpha_R(1 - e^{ik}) & B \cos(\theta) - M & 1 + e^{ik} & -B \sin(\theta) - \Delta \end{pmatrix}$$

and  $H_- = -H_+$  after a unitary transformation

$$U = \frac{1}{\sqrt{2}} \begin{pmatrix} 1 & 0 & 0 & 0 & 0 & 0 & -1 & 0 \\ 0 & 1 & 0 & 0 & 0 & 0 & 0 & 1 \\ 0 & 0 & 1 & 0 & 1 & 0 & 0 & 0 \\ 0 & 0 & 0 & 1 & 0 & -1 & 0 & 0 \\ 0 & 0 & -1 & 0 & 1 & 0 & 0 & 0 \\ 0 & 0 & 0 & 1 & 0 & 1 & 0 & 0 \\ 1 & 0 & 0 & 0 & 0 & 0 & 1 & 0 \\ 0 & -1 & 0 & 0 & 0 & 0 & 0 & 1 \end{pmatrix}$$

So when  $\mu = 0$ , phase transition happens at the points  $M^2 = B^2 \cos(2\theta) + \Delta^2 - 4 \pm 2\sqrt{-B^4 \cos^2(\theta) \sin^2(\theta) + B^2 \Delta^2 \cos^2(\theta) + 4B^2 \sin^2(\theta) - 4\Delta^2}$  and  $M^2 = B^2 \cos(2\theta) + 4\alpha_R^2 + \Delta^2 - 2B\sqrt{-B^2 \cos^2(\theta) \sin^2(\theta) + \Delta^2 \cos^2(\theta) - 4\alpha_R^2 \sin^2(\theta)}$ .

In Fig. 7 we plot the energy spectrum for a chain with open boundary condition (left column) and for a ring with one AF domain-wall on it (right column). Like that in the first model, the AF domain-wall is simulated by two adjacent  $M_i$ s pointing to the same direction. We find in the cases (c), (d), (e) and (f), there is a TSP in which a MF zero energy bound state can coexist with a JRBS. These properties are the same as those showed for the first model.

We also numerically calculate the electric charge carried by an AF domain-wall. As Fig. 8 shows, it is non-universal just as that in the first model. We also numerically calculate the parities of fermion numbers for chains like A and B. The result is same as that in the first model. So the JRBS attached to the AF domain-wall in this model is also carrying FP.

---

<sup>1</sup> J. P. Hague and C. MacCormick, New J. of Phys. **14**, 033019 (2012).

<sup>2</sup> M. Atala and et. al., arXiv:1212.0572 (2012).

- <sup>3</sup> X.-J. Liu, T. Law, K., and K. Ng, T., Phys. Rev. Lett. **112**, 086401 (2014).
- <sup>4</sup> H. Lu, L. O. Baksmaty, C. J. Bolech, and H. Pu, Phys. Rev. Lett. **108**, 225302 (2012).
- <sup>5</sup> Y. Xu, R.-L. Chu, and C. Zhang, Phys. Rev. Lett. **112**, 136402 (2014).
- <sup>6</sup> P. Fulde and R. A. Ferrell, Phys. Rev. **135**, A550 (1964).
- <sup>7</sup> C. Chen, Phys. Rev. Lett. **111**, 235302 (2013).
- <sup>8</sup> J. C. Budich and E. Ardonne, Phys. Rev. B **88**, 075419 (2013).
- <sup>9</sup> E. Gaidamauskas, J. Paaske, and K. Flensberg, Phys. Rev. Lett. **112**, 126402 (2014).
- <sup>10</sup> A. Haim, A. Keselman, E. Berg, and Y. Oreg, Phys. Rev. B **89**, 220504 (2014).
- <sup>11</sup> X. Ye and T. Peiqing, arXiv:1406:5568.

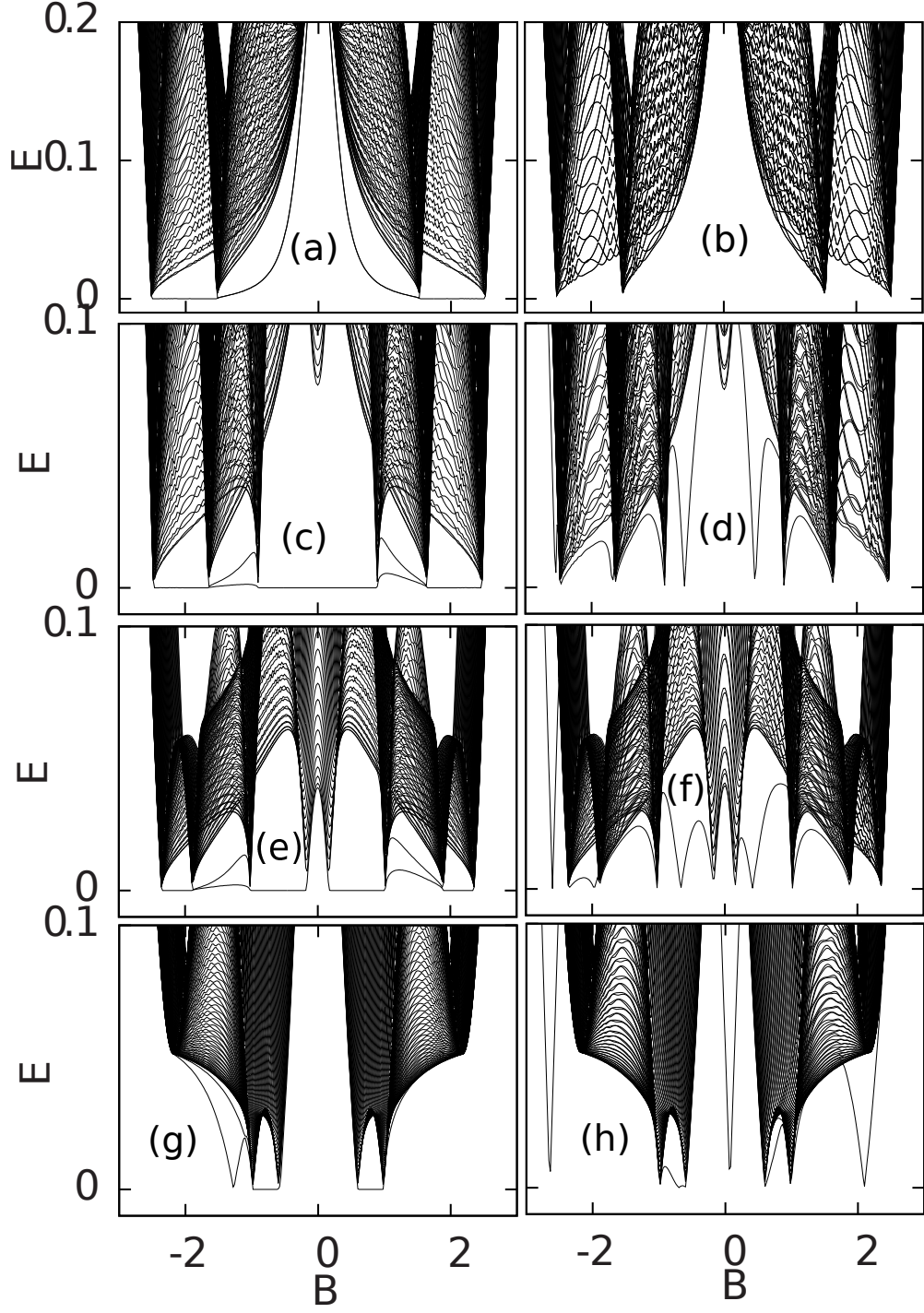


FIG. 7: The energy spectrum for a  $N = 400$  chain with open boundary condition (left column) and for a  $N = 401$  ring with an AF domain-wall (right column). The parameters are  $\theta = 0.6$ ,  $\Delta = 0.3$  and  $\alpha_R = 0.1$  in these panels.  $M$  is 0 (a) (b), 0.5 (c) (d), 0.8 (e) (f) and 1 (g) (h).

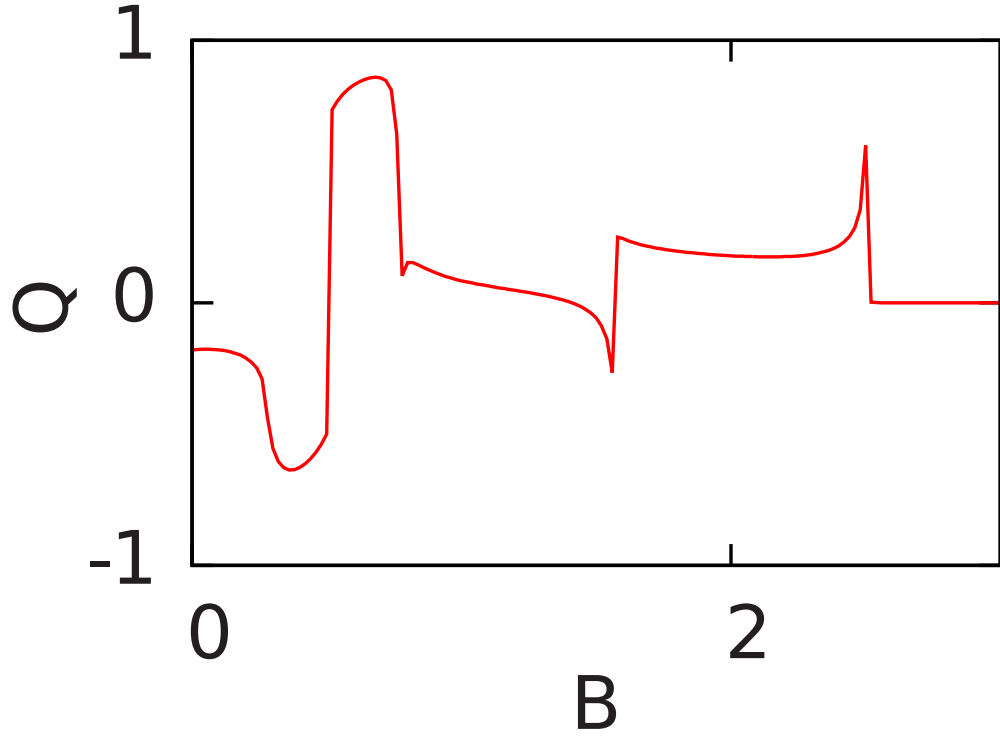


FIG. 8: The electric charge carried by an AF domain-wall. The parameters are  $\theta = 0.6$ ,  $\Delta = 0.3$ ,  $\alpha_R = 0.1$  and  $M = 0.2$ .